Eur. Phys. J. B **53**, 169–184 (2006)
DOI: 10.1140/epjb/e2006-00367-6

THE EUROPEAN PHYSICAL JOURNAL B

X-ray detected ferromagnetic resonance in thin films

Uniform precession in a steady-state foldover regime

J. Goulon[1], A. Rogalev[1], F. Wilhelm[1], N. Jaouen[1], C. Goulon-Ginet[1], and Ch. Brouder[2]

[1] European Synchrotron Radiation Facility, B.P. 220, 38043 Grenoble Cedex, France
[2] Laboratoire de Minéralogie-Cristallographie, UMR-CNRS 7590, Université Paris VI-VII, IPGP, 4 place Jussieu, 75252 Paris Cedex 05, France

Received 5 May 2006 / Received in final form 28 August 2006
Published online 6 October 2006 –

Abstract. We discuss the physical content of X-ray Detected Magnetic Resonance (XDMR), i.e. a novel spectroscopy which uses XMCD to probe the resonant precession of the local magnetization in a strong microwave pump field. We focus on the simplest case of a steady-state precession of elemental moments in the non-linear regime of angular foldover. Like XMCD, XDMR is element and edge selective and could become a unique tool to investigate how precessional dynamics can locally affect the spin and orbital magnetization of *p*- or *d*-projected DOS. This should be possible only in the limit where there is no overdamping due to ultrafast orbit-lattice relaxation.

PACS. 78.70.Dm X-ray absorption spectra – 78.20.Ls Magnetooptical effects – 76.20.+q General theory of resonances and relaxations – 76.50.+g Ferromagnetic, antiferromagnetic, and ferrimagnetic resonances; spin-wave resonance

1 Introduction

X-ray Magnetic Circular Dichroism (XMCD) has become an important tool to study orbital magnetism [1]. XMCD benefits of the unique advantage to be element/edge selective and became particularly attractive when the magneto-optical sum-rules at spin-orbit split edges made it possible to resolve the individual contributions of spin and orbital moments at different sites [1–5]. Further information regarding the dynamics of magnetization reversal at a subnanosecond time scale was already obtained from pioneering XMCD experiments exploiting the time structure of the ESRF storage ring [6]. We are concerned below with a different approach of magnetization dynamics: X-ray Detected Magnetic Resonance (XDMR) is a novel spectroscopy in which XMCD is used to probe *locally* the resonant precession of the magnetization caused by a strong microwave pump field. XDMR is thus a transposition into the X-ray regime of Optically Detected Magnetic Resonance (ODMR) [7–10].

Very recently, precessional motions of elemental spin moments were observed by Bailey et al. [11] who combined time-resolved soft X-ray differential circular reflectometry with Pulsed Induction Magnetometry (PIM). This is an alternative approach to the same physics even though time-domain measurements are restricted to low frequency resonances. At the ESRF, time and efforts were invested for several years on detecting XDMR in the *frequency domain* [12]. Two experiments were run on Yttrium Iron Garnet (YIG): (i) the first one at the L-edges of iron [13] was a feasibility test; (ii) a more challenging experiment was carried out at the iron K-edge with a high quality thin film epitaxially grown on a Gadolinium Gallium Garnet (GGG) substrate. The latter experiment produced the first direct evidence of the forced precession of magnetically polarized *orbital* components [14]. The possibility to image ferromagnetic resonance eigenmodes was also demonstrated by Puzic et al. [15] who, again, used soft-XMCD as a probe.

As illustrated with Figure 1, two complementary geometries can be envisaged to measure a XDMR signal in a ferromagnetic thin film magnetized perpendicularly:

(i) In the *longitudinal* geometry, the wavevector $\mathbf{k_x}$ of the incident, circularly polarized X-rays is parallel to the static magnetic field $\mathbf{H_0}$, whereas the microwave pump field $\mathbf{h_p}$ is perpendicular to $\mathbf{H_0}$ which is arbitrarily taken here to coincide with the direction of the equilibrium magnetization. If one assumes that the length of the equilibrium magnetization (M_s) is invariant in the precession, there should be along the direction of $\mathbf{H_0}$ a time-invariant change in the magnetization (ΔM_z) that could be probed with XMCD.
(ii) In the *transverse* geometry, the wavevector $\mathbf{k_x}$ is perpendicular to both $\mathbf{H_0}$ and $\mathbf{h_p}$: the precession of the magnetic moments would now induce a larger XMCD signal proportional to $\Delta M_\perp$ but oscillating at the microwave resonance frequency.

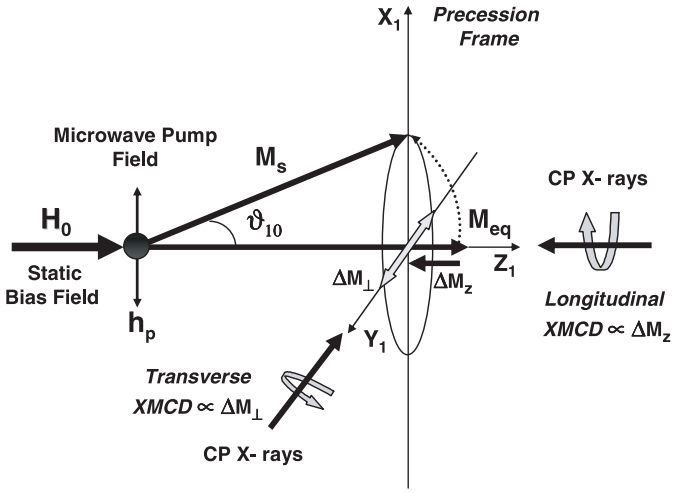

Fig. 1. XDMR in *Longitudinal* or *Transverse* geometries. Note the time-invariant character of the XMCD signal due to ΔM_Z.

Obviously, the detection of the XDMR signal in the transverse geometry requires a fast X-ray detector and a very sophisticated electronics. What makes the longitudinal geometry particularly attractive is precisely the argument that no fast X-ray detector is needed because the XDMR signal will be shown to be proportional to the microwave *power* which can be amplitude modulated at low frequency.

In Section 2, we review the conceptual bases of a simple interpretation of X-ray detected FMR in the uniform mode. We focus onto the regime of *steady-state* precession caused by a strong microwave field in a ferromagnetic thin film magnetized perpendicularly to the film. We examine carefully the approximations required for this model to be valid but, for conciseness, we defer to a forthcoming paper a more detailed analysis of XDMR in the regime of elliptical precession with harmonic generation [19]. Other effects related to non-uniform precession, e.g. longitudinal pumping and parametric amplification of magneto-exchange modes in metallic thin films are left beyond the scope of this paper. Let us emphasize that the very weak intensity of the XDMR signals makes large precession angles highly desirable, which is possible only with strong microwave fields. In this respect, it is noteworthy that Bloembergen and co-workers [16–18] were the first to recognize long time ago that the longitudinal geometry was much less sensitive to magnon-magnon scattering processes and had a much higher saturation limit regarding the incident microwave power. Non-linear effects, however, cannot be neglected at high pumping power [18] and are known to cause spectacular *foldover* effects in ferromagnets featuring a large anisotropy [20–22].

In Section 3, XDMR will be shown to probe *locally*, i.e. at the X-ray absorbing sites, a time-averaged precession cone for selected magnetization components. We compare what is the relevant information to be extracted from XDMR spectra recorded at a photoionization K-edge or at spin-orbit split L-edges. Extended sum rules for XDMR are considered. In this context, the old concept of fictitious spin Hamiltonians may have to be revisited to make allowance for crystal field and spin-orbit splitting [23–26] and to analyze orbit-lattice relaxation mechanisms [27].

2 Uniform mode of precession

2.1 Equations of motion

For any elemental magnetization vector $\mathbf{M}(\mathbf{r},t)$, one can deduce the following equation of motion from the conservation of spin or angular momentum [28,31]:

$$\frac{\partial \mathbf{M}(\mathbf{r},t)}{\partial t} = -\gamma \mathbf{T}(\mathbf{r},t) = -\gamma \mathbf{M} \times \mathbf{B_e} \tag{1}$$

where $\gamma = g\mu_B/\hbar$ denotes the gyromagnetic ratio. It was recognized by Landau and Lifshitz that equation (1) described a precession of the magnetization vector $\mathbf{M}$ around an effective, instantaneous field $\mathbf{B_e}(\mathbf{r},t)$ defined as the functional derivative of the free energy (F) with respect to the magnetic moment $\mathbf{M}(\mathbf{r},t)$ [28]:

$$\mathbf{B_e}(\mathbf{r},t) = \mu_0 \mathbf{H_e}(\mathbf{r},t) = -\frac{\delta F}{\delta \mathbf{M}(\mathbf{r},t)}. \tag{2}$$

In equation (1), $\mathbf{T}(\mathbf{r},t)$ is the total torque acting on $\mathbf{M}(\mathbf{r},t)$: it includes contributions from external and internal magnetic fields. External fields encompass both the static (bias) field $\mathbf{H_0}$ and the microwave (pump) field $\mathbf{h_p}$. Internal fields include the exchange field $\mathbf{H}_{ex}$, the demagnetizing field $\mathbf{H}_D$ due to long range dipolar interactions and the magnetic anisotropy field $\mathbf{H}_A$ which results from miscellaneous contributions due to dipolar and spin-orbit interactions. The exchange field $\mathbf{H}_{ex}$ combines terms proportional to both $\mathbf{M}$ and $\nabla^2\mathbf{M}$ but equation (1) implies that only the inhomogeneous exchange term ($\nabla^2\mathbf{M}$) could contribute to a non-vanishing torque since $\mathbf{M} \times \mathbf{M} \equiv 0$. Even though the spectroscopic splitting factor g should be a tensor property like in EPR [29], it will be taken below as a scalar since we are concerned in this paper with the precession of spin and orbital magnetization components around one well defined crystal direction.

A phenomenological damping torque is usually added which drives the magnetization $\mathbf{M}$ back towards the equilibrium state with $\mathbf{M}_{eq}$ parallel to $\mathbf{H_e}$. In the original Landau-Lifshitz's formulation (LL), the damping torque was written [21,32–34]:

$$\mathbf{T}_{LL} = +\frac{\omega_{LL}}{\gamma M_s^2}[\mathbf{M} \times (\mathbf{M} \times \mathbf{B_e})] \tag{3}$$

where M_s is the saturation magnetization and ω_{LL} is a relaxation frequency. Since $[\mathbf{M} \times (\mathbf{M} \times \mathbf{B_e})]$ is perpendicular to $\mathbf{M}$, $\mathbf{T}_{LL}$ can change the direction but *not* the magnitude of $\mathbf{M}$ [21]. The Landau-Lifshitz-Gilbert (LLG)

formulation is often preferred because it does not depend anymore on the effective field $\mathbf{B_e}$ [21]:

$$\mathbf{T}_{LLG} = +\frac{\alpha}{\gamma M_s}\mathbf{M} \times \frac{\partial \mathbf{M}}{\partial t} \tag{4}$$

$\alpha = \omega_{LL}/\gamma M_s$ being here a dimensionless, scalar constant. Both formulations (LL or LLG) were shown to be strictly equivalent if one replaces γ with $\gamma* = \gamma(1+\alpha^2)$ in equation (1) [30]. A formal analogy was alleged between the Gilbert damping and a magnetic viscosity [33]. It is noteworthy that the LLG formulation is fully consistent with the fluctuation-dissipation theorem [35], while this is not the case for the Bloch-Bloembergen (BB) torque: $\mathbf{T}_{BB} = (\omega_r/\gamma)[\mathbf{M} - \mathbf{M}_{eq}]$ which does not conserve anymore the length of $\mathbf{M}$ [21]. To make it consistent with the fluctuation-dissipation theorem, $\mathbf{T}_{BB}$ has to be modified according to a prescription proposed by Wangsness [36]:

$$\mathbf{T}_{BBW} = +\frac{\omega_r}{\gamma}\left[\mathbf{M} - \frac{M_s}{H_{eq}}\mathbf{H_e}\right]. \tag{5}$$

In equation (5) ω_r is again a relaxation frequency, H_{eq} being the effective equilibrium field in the absence of microwaves. The key difference with respect to the BB formulation is that relaxation is now directed towards the instantaneous effective field $\mathbf{H_e}$. The BB equation of motion and its BBW modified form, are most often associated with two distinct relaxation times [17,37]: a longitudinal relaxation time T_1 parallel to the direction of $\mathbf{H_0}$ and a transverse relaxation time T_2 perpendicular to the direction of $\mathbf{H_0}$. This is attractive because T_2 is more sensitive to random processes that couple the uniform mode ($\mathbf{k} = 0$) to thermally excited magneto-exchange modes or spin-waves ($\mathbf{k} \neq 0$) [37]. On the other hand, Callen and his colleagues [38,39] pointed out that, even the simplest damping torque model for magnon scattering ($\mathbf{T}_{MS}$) would require the definition of at least three kinetic parameters:

$$\mathbf{T}_{MS} = -\frac{(\lambda_{0k} + \lambda_{0\sigma})}{2H_0^2}[\mathbf{H_0} \times (\mathbf{M} \times \mathbf{H_0})] + [\lambda_{k\sigma}(M_{eq} - M) + \frac{\lambda_{0\sigma}}{H_0}(MH_0 - \mathbf{M}.\mathbf{H_0})]\mathbf{H_0}/H_0. \tag{6}$$

Here, λ_{0k} is the probability of destruction of a $k = 0$ magnon with the simultaneous production of a $k \neq 0$ magnon, and $\lambda_{0\sigma}$ and $\lambda_{k\sigma}$ are the probabilities of disappearance of $k = 0$ and $k \neq 0$ magnons respectively. Numerous theories of FMR relaxation aimed at calculating the various λ_{ij}. Both crystal field and spin-orbit interaction will affect the calculation of λ_{0k} [38] and could cause a marked orientational anisotropy of the FMR linewidth ΔH as observed experimentally [38–40]. In Section 2.5, the FMR linewidth ΔH will allow us to switch from one damping model to another. Fletcher et al. [37] made, however, the interesting remark that, even though it is inapplicable to the *average* magnetization measured in standard FMR experiments, the LLG equation should be a reasonable approximation on the *microscopic scale* relevant to XDMR which is a local probe.

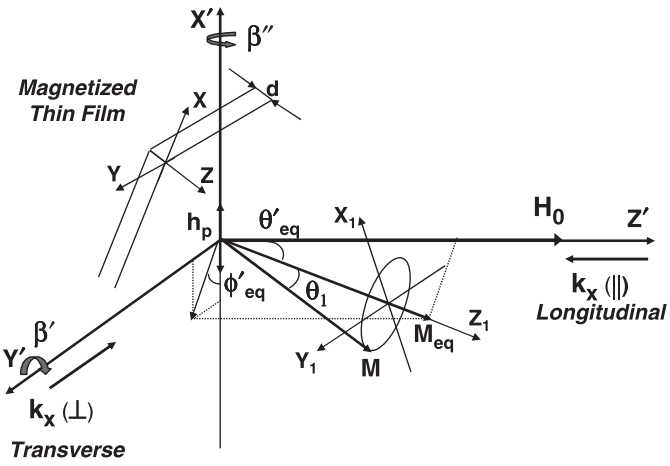

Fig. 2. XDMR reference frames: The equilibrium magnetization $\mathbf{M_{eq}}(\theta'_{eq}, \phi'_{eq})$ refers to the laboratory frame $(\mathbf{x}', \mathbf{y}', \mathbf{z}')$. $\mathbf{M}(\theta_1, \phi_1)$ defines the precessing magnetization in the precession frame $(\mathbf{x_1}, \mathbf{y_1}, \mathbf{z_1})$. Usually, $\mathbf{M_{eq}}$ is not rigorously parallel to the external static bias field $\mathbf{H_0}$.

2.2 Small amplitude precession: linear FMR regime

It is most convenient to define the magnetization vector $\mathbf{M}$ by its polar and azimuthal angles (θ, ϕ) and its norm M. As illustrated with Figure 2, three different coordinate systems will be considered throughout this paper: (i) $\mathbf{M}(\theta, \phi)$ will refer to the symmetry axes (X, Y, Z) of a film grown along the direction Z; (ii) $\mathbf{M}(\theta', \phi')$ will refer to the laboratory frame (X', Y', Z') in which the external fields $\mathbf{H_0}, \mathbf{h_p}$ and the X-ray wavevector $\mathbf{k_x}$ are defined; (iii) finally, $\mathbf{M}(\theta_1, \phi_1)$ will refer to the *precession* frame (X_1, Y_1, Z_1) with Z_1 directed along the direction of the equilibrium magnetization $\mathbf{M}_{eq}$ which, very often, does not coincide with the direction of $\mathbf{H_0}$.

In the absence of damping, Leeuw et al. [31] noted that the torque acting on $\mathbf{M}(\theta', \phi')$ could be split into well identified contributions:

$$\mathbf{T_i} = \frac{1}{M_s \sin\theta'}\frac{\delta F_i}{\delta \phi'}\frac{\partial \mathbf{M}}{\partial \theta'} - \frac{1}{M_s \sin\theta'}\frac{\delta F_i}{\delta \theta'}\frac{\partial \mathbf{M}}{\partial \phi'}$$

in which $F_i(\theta', \phi', \nabla\theta', \nabla\phi', \mathbf{r}, t)$ would refer to the Zeeman free energy F_Z, a demagnetizing term F_D and a magnetic anisotropy free energy F_A.

If one assumes that the sample is single domain biased and that $\mathbf{M}(\theta', \phi')$ is uniform all over the sample, then there is no contributing torque left from inhomogeneous exchange [21,28], whereas partial derivatives can replace functional derivatives. Since the demagnetizing energy depends on the shape of the sample, we shall restrict our analysis to the case of infinite thin films, i.e. slabs with a vanishing aspect ratio. To further compact notations, F_{AD} will regroup hereafter the magnetic anisotropy free energy F_A plus the demagnetizing energy F_D. Then, the

LLG equations can be rewritten [21,41]:

$$(1+\alpha^2)\frac{d\theta'}{dt} = -\frac{\gamma}{M_s}\left(\alpha\frac{\partial F}{\partial\theta'} + \frac{1}{\sin\theta'}\frac{\partial F}{\partial\phi'}\right) \quad (7)$$

$$(1+\alpha^2)\frac{d\phi'}{dt} = +\frac{\gamma}{M_s}\left(\frac{1}{\sin\theta'}\frac{\partial F}{\partial\theta'} - \frac{\alpha}{\sin^2\theta'}\frac{\partial F}{\partial\phi'}\right) \quad (8)$$

where $F = F_Z(\theta',\phi') + F_{AD}(\theta',\phi')$. Another equation has still to be added if one decides to use the BBW formalism because the length of the magnetization vector (M) is not anymore invariant:

$$\frac{\partial M}{\partial t} = -\omega_r\left[\frac{M_s}{H_{eq}}\frac{\partial F}{\partial M} - M\right]. \quad (9)$$

The direction around which $\mathbf{M}$ will precess is defined by the equilibrium condition: $\partial F/\partial\theta' = 0 = \partial F/\partial\phi'$. It is usually impossible to evaluate $(\theta'_{eq},\phi'_{eq})$ in closed form and one has to resort to numerical methods [42]. Anyhow, the amount of algebra can be reduced if one selects symmetry coordinates. Let $\mathbf{M}(\theta,\phi)$ refer to such coordinates and let us expand the magnetic anisotropy free energy $F_{AD}(\theta,\phi)$ on a basis of real spherical harmonics:

$$F_{AD}(\theta,\phi) = \sum_{\ell,m} A'_{\ell m}u_{\ell m}(\theta,\phi) + A''_{\ell m}v_{\ell m}(\theta,\phi)$$

in which $m \geq 0$ and:

$$u_{\ell m}(\theta,\phi) = \frac{1}{2}[C_{\ell m}(\theta,\phi) + (-1)^m C_{\ell -m}(\theta,\phi)]$$

$$v_{\ell m}(\theta,\phi) = \frac{1}{2i}[C_{\ell m}(\theta,\phi) - (-1)^m C_{\ell -m}(\theta,\phi)]$$

$C_{\ell m}$ denoting normalized spherical harmonics [43]. The coefficients $A'_{\ell m}$ and $A''_{\ell m}$ are listed in Appendix A for a variety of films with either uniaxial or cubic magnetic anisotropy. Transformations from symmetry coordinates towards laboratory coordinates are considered in Appendix B. Conversely, starting with the static Zeeman free energy in the laboratory coordinates:

$$F_Z(B_0) = -M_sB_0\cos\theta' = -M_sB_0C_{10}(\theta',\phi')$$

one may transpose it into the sample coordinates (X,Y,Z) if the polar and azimuthal angles (θ_H,ϕ_H) of the static field $\mathbf{H_0}$ are known in this new coordinates system:

$$F_Z(B_0) = -M_sB_0[C_{10}(\theta_H,\phi_H)C_{10}(\theta,\phi) + 2u_{11}(\theta_H,\phi_H)u_{11}(\theta,\phi) + 2v_{11}(\theta_H,\phi_H)v_{11}(\theta,\phi)].$$

In practice, one may often identify elementary rotations (e.g. β' or β'') transforming the laboratory coordinates into the sample symmetry coordinates. For example, let us consider a YIG film grown on a (111) GGG substrate and let us assume that it is inclined by a tilt angle $\beta'_N = -30°$ just as reported in the XDMR experiment of reference [14]: $\theta_H = -\beta'_N$ and $\phi_H = 0$. Neglecting any cubic anisotropy, the equilibrium condition is:

$$\frac{\sin(\theta_{eq}-\theta_H)}{\sin 2\theta_{eq}} = -\frac{1}{2}\frac{B_u}{B_0} \simeq \frac{3}{2}\frac{A'_{20}}{M_sB_0} \quad (10)$$

in which B_u is the uniaxial anisotropy field defined as: $B_u = 2K_{u1}/M_s - \mu_0 DM_s$ (in SI units). Within this definition, K_{u1} is the first order uniaxial anisotropy constant, the effective demagnetizing factor D being unity only for a film of vanishing aspect ratio [34,40]. Equation (10) implies that $\phi_{eq} = 0$ whereas $\theta_{eq} = 0$ only if $\theta_H = 0$. Typically, if $\beta'_N = -30°$, $B_u = -165$ mT and $B_0 = 424.13$ mT, one obtains $\theta_{eq} = 35.28°$ or $\theta'_{eq} = \theta_{eq} - \theta_H = 5.28°$. The higher the microwave frequency will be, the higher the static resonance field B_0 will also be, and, consequently, the smaller θ'_{eq} will be.

Introducing a cubic anisotropy field $B_{A1} = 2K_1/M_s$ does not add any difficulty as long as one neglects all terms which break cylindrical symmetry ($A'_{\ell m}$, $A''_{\ell m}$ with $m \neq 0$). For a YIG film grown on a (111) substrate, there is such a weak trigonal term (A''_{43}) yielding:

$$\frac{\sin(\phi_H-\phi_{eq})}{\cos 3\phi_{eq}} \simeq \frac{\sqrt{2}}{4}\frac{B_{A1}}{B_0}\sin 2\theta_H \times\left[1 + \frac{\sin(\theta_{eq}-\theta_H)}{\sin 2\theta_H}(1+3\cos 2\theta_H) + ...\right]. \quad (11)$$

With B_{A1} of the order of 5 mT, the perturbation remains very small and $\phi'_{eq} = \phi_{eq} \simeq 0.26°$ for $\phi_H = 0$. For the general case, a computer code makes it a trivial task to determine the equilibrium direction for any ferromagnetic film featuring common cubic symmetries.

In the *linear regime* of FMR, the Smit-Beljers-Suhl (SBS) formula [44,45] determines the eigen-frequency ω_0 of the system, i.e. the FMR resonance frequency *without* microwave field nor damping torque. It is classically derived by solving the LLG using a Taylor series expansion of the total free energy density for small angular deviations from the equilibrium values, i.e. $\delta\theta = \theta - \theta_{eq}$ and $\delta\phi = \phi - \phi_{eq}$. This led to the well-known result:

$$\omega_0 = \frac{\gamma}{M_s\sin\theta_{eq}}[F_{\theta\theta}F_{\phi\phi} - (F_{\theta\phi})^2]^{1/2}. \quad (12)$$

Here, $F_{\theta\theta}$, $F_{\phi\phi}$ and $F_{\theta\phi}$ are short notations for the 2nd derivatives of the free energy and describe the *magnetic stiffness* along the equilibrium direction (θ_{eq},ϕ_{eq}). As noted by several authors ([21,42]), equation (12) is singular for $\theta_{eq} = 0$ and cannot be used for a ferromagnetic film with perpendicular magnetization as primarily considered in Figure 1. Equation (12), however, is most convenient for a film slightly inclined or rotated (β', $\beta'' \neq 0$).

Energy dissipation can be taken into account with a complex resonance frequency ω^*_R. Following Skrotskii and Kurbatov [46], one would get for the real part: $\omega'_R = \omega_0(1+\alpha^2)^{1/2}$, and for the imaginary part:

$$\omega''_R = \frac{1}{2}\Delta\omega_0 = \frac{1}{2}\frac{\alpha\gamma}{M_s}\left[F_{\theta\theta} + \frac{1}{\sin^2\theta_{eq}}F_{\phi\phi}\right] \quad (13)$$

in which $\Delta\omega_0 = \gamma\Delta H$ is the FMR linewidth. A similar formulation was already included in Suhl's original paper [45]. The practical value of equation (13) is difficult to assess for a slightly inclined film because additional

(anisotropic) relaxation processes such as magnon scattering may become activated as well. Frequency dependent FMR measurements may not be sufficient to discriminate unambiguously a true Gilbert damping process against other relaxation processes which may exhibit as well a linear frequency dependence of their contribution to the FMR linewidth [47].

2.3 Large amplitude precession: XDMR regime

In the precession frame (X_1, Y_1, Z_1), $\mathbf{M}(\theta_1, \phi_1)$ deviates only slightly from the equilibrium position: $\theta_{1eq} = 0$. Following Gurevich [21], we seek the solution of the equation of motion in the form:

$$\mathbf{M} = \mathbf{M}_{eq} + \mathbf{\Delta M}^{(1)} + \mathbf{\Delta M}^{(2)} + ... \qquad (14)$$

in which $\mathbf{\Delta M}^{(1)} \ll \mathbf{M}_{eq}$, whereas $\mathbf{\Delta M}^{(2)} \ll \mathbf{\Delta M}^{(1)}$, $\mathbf{\Delta M}^{(n)}$ with $n \geq 2$ referring to weak high-order nonlinear magnetic susceptibilities. Let $\mathbf{\Delta M}_\perp$ denote the projection of $[\mathbf{\Delta M}^{(1)} + \mathbf{\Delta M}^{(2)} + ...]$ in the plane (X_1, Y_1). It is anticipated that $\mathbf{\Delta M}^{(2)}$, which is oriented mainly along Z_1 for a weakly elliptical precession, will have only a small contribution to $\mathbf{\Delta M}_\perp$ [18,21]. Forced precession occurs whenever the azimuthal angle of $\mathbf{\Delta M}_\perp$ satisfies the resonance condition:

$$\phi_1 = \phi^{(1)} + \Delta\phi^{(n)} = \omega t + \phi_{1_0} + \Delta\phi^{(n)}. \qquad (15)$$

Here $\Delta\phi^{(n)}$ is accounting for the very weak phase modulation due to the generic high order phasor: $\Delta M_\perp^{(n)} e^{i\phi^{(n)}}$. Defining next: $\delta\phi^{(n)} = \phi^{(n)} - \phi^{(1)}$, one would easily show that, to the lowest approximation,

$$\Delta\phi^{(n)} \simeq \rho_\perp^{(n)} \sin\delta\phi^{(n)} + ... \text{ with:}$$
$$\rho_\perp^{(n)} = [\Delta M_\perp^{(n)}]/[\Delta M_\perp^{(1)}] \ll 1.$$

Note that we will make use below of the extended time-derivative: $\tilde{\omega} = d\phi_1/dt = \omega + \Delta\dot{\phi}^{(n)}$.

It is often postulated that the microwave pump field $b_p = \mu_0 h_p$ is circularly polarized in the (X', Y') plane. In a real experiment, it is most frequently linearly polarized (b_{lp}). If we assume that it oscillates along X', then the time-dependent part of the Zeeman free energy can be written as:

$$F_Z(b_{lp}) = \frac{\sqrt{2}}{2} M_s b_{lp} [u_{11}(\theta', \phi' - \omega t) + u_{11}(\theta', \phi' + \omega t)].$$

Again the Wigner D-functions $D^\ell_{mn}(\alpha'_0, \beta'_0, \gamma'_0)$ provide us with a simple way to calculate $F_Z(\theta_1, \phi_1)$ since:

$$C_{\ell m}(\theta', \phi') = \sum_n D^{*\ell}_{mn}(\alpha'_0, \beta'_0, \gamma'_0) C_{\ell n}(\theta_1, \phi_1) \qquad (16)$$

Here $(\alpha'_0 = \phi'_{eq}, \beta'_0 = \theta'_{eq}, \gamma'_0 = 0)$ is an Eulerian rotation transforming the laboratory frame (X', Y', Z') into the precession frame (X_1, Y_1, Z_1). The determination of θ'_{eq} and ϕ'_{eq} was already discussed in Section 2.2. For the trivial case of a ferromagnetic film with uniaxial symmetry and perpendicular magnetization, equation (16) is not needed since $\theta'_{eq} = \phi'_{eq} = 0$. It is required either when the magnetic anisotropy has no cylindrical symmetry, or when the film is slightly inclined (β'_N). In the latter case, we found $\theta'_{eq} = \theta_{eq} + \beta'_N$ with $\phi'_{eq} = \phi_{eq} \simeq 0$.

The Zeeman free energy $F_Z(\theta_1, \phi_1)$ can be split into a static term due to the bias field $\mathbf{B}_0$, a steady-state term due to the pump field $\mathbf{b}_p$, plus two contributions oscillating at ω and 2ω respectively:

$$F_Z = F_Z^{(0)}(B_0) + F_Z^{(0)}(b_p) + \Delta F_Z^{(1)}(\omega t) + \Delta F_Z^{(2)}(2\omega t)$$

with the identification:

$$F_Z^{(0)}(B_0) = -M_s B_0 \cos\beta'_0 \cos\theta_1$$

$$F_Z^{(0)}(b_{lp}) = -\frac{1}{2} M_s b_{lp} \sin\theta_1 \times [\cos\beta'_0 \cos\alpha'_0 \cos\psi_1 - \sin\alpha'_0 \sin\psi_1]$$

$$\Delta F_Z^{(1)}(B_0, b_{lp}; \omega t) = M_s \cos\alpha'_0 \sin\beta'_0 \times [B_0 \sin\theta_1 \cos(\omega t + \psi_1) - b_{lp} \cos\theta_1 \cos\omega t]$$

$$\Delta F_Z^{(2)}(b_{lp}; 2\omega t) = -\frac{1}{2} M_s b_{lp} \sin\theta_1 \times [\cos\beta'_0 \cos\alpha'_0 \cos(2\omega t + \psi_1) - \sin\alpha'_0 \sin(2\omega t + \psi_1)]$$

in which: $\psi_1 = \phi_{1_0} + \Delta\phi^{(n)} + \gamma'_0$. It appears that $\Delta F_Z^{(1)} \propto \sin\beta'_0$. Since $\beta'_0 \to 0$ for a ferromagnetic film magnetized perpendicularly, $\Delta F_Z^{(1)}$ should vanish or play only a minor role when the film is slightly tilted. This is not true for $\Delta F_Z^{(2)}$ which has long been recognized to contribute to harmonic generation.

We noted in Section 2.2 that F_{AD} should preferably be expressed in the sample symmetry coordinates. We simply need to replace $(\alpha'_0, \beta'_0, \gamma'_0)$ in equation (16) with $(\alpha_0, \beta_0, \gamma_0)$, i.e. the Eulerian rotation transforming the sample symmetry axes (X, Y, Z) into the precession frame (X_1, Y_1, Z_1). Indeed: $\alpha_0 = \phi_{eq}$, $\beta_0 = \theta_{eq}$ and $\gamma_0 = 0$.

The LLG equations can then be reformulated as:

$$-\frac{1}{M_s \sin\theta_1} \frac{\partial}{\partial\theta_1} [F_Z^{(0)}(b_p) + \Delta F_Z^{(2)}(b_p)] = P_1/\gamma \qquad (17)$$

$$+\frac{1}{M_s \sin^2\theta_1} \frac{\partial}{\partial\phi_1} [F_Z^{(0)}(b_p) + \Delta F_Z^{(2)}(b_p)] = Q_1/\gamma \qquad (18)$$

in which we introduced the notations:

$$P_1 = -\tilde{\omega} + \frac{\gamma}{M_s \sin\theta_1} \frac{\partial}{\partial\theta_1} F_Z^{(0)}(B_0) + \frac{\gamma}{M_s \sin\theta_1} \frac{\partial}{\partial\theta_1} [F_{AD} + \Delta F_Z^{(1)}(B_0, b_p)] + \frac{\alpha\dot{\theta_1}}{\sin\theta_1} \qquad (19)$$

$$Q_1 = -\alpha\tilde{\omega} - \frac{\gamma}{M_s \sin^2\theta_1}\frac{\partial}{\partial\phi_1}[F_{AD} + \Delta F_Z^{(1)}(B_0, b_p)] - \frac{\dot{\theta_1}}{\sin\theta_1}. \quad (20)$$

Equations (17, 18) lead to the formal result:

$$\tan^2\theta_1[P_1^2 + (Q_1\cos\theta_1)^2] = N_p^2 \quad (21)$$

For a linearly polarized microwave field:

$$N_{lp}^2 = \frac{1}{2}(\gamma b_{lp})^2[\cos^2\beta_0'\cos^2\alpha_0' + \sin^2\alpha_0'](1+\cos 2\omega t)$$

which reduces to:

$$N_{lp_0}^2 = \frac{1}{4}(\gamma b_{lp})^2[\cos^2\beta_0'\cos^2\alpha_0' + \sin^2\alpha_0'] = \frac{1}{4}(\gamma b_{lp})^2[1-\epsilon_{lp}]$$

if one neglects $\Delta F_Z^{(2)}$ in equations (17, 18). Keeping in mind that (α_0',β_0',γ_0') are vanishingly small angles for ferromagnetic films with uniaxial anisotropy and perpendicular magnetization, we expect $\epsilon_{lp} \to 0$. Only in this limit is a linearly polarized microwave field strictly equivalent to a circularly polarized field of half strength. Typically, with $\beta_N' = -30°$ and $\beta_0' = \theta_{eq}' \simeq 5.28°$, $\epsilon_{lp} \leq 0.008$.

Another quantity of interest is: $\tan\Psi_1 = Q_1\cos\theta_1/P_1$. For a linearly polarized microwave field, one obtains: $\Psi_1 = \psi_1 + \chi_{lp}$, with $\tan\chi_{lp} = \tan\alpha_0'/\cos\beta_0'$ in which: $\chi_{lp} \to 0$ for YIG films.

2.4 Steady-state precession: foldover regime

In practice, equation (21) cannot be exploited unless a strategy is elaborated to calculate the time-derivatives $\tilde{\omega}$ and $\dot{\theta_1} = d\theta_1/dt$. The *steady-state* approximation refers to a drastic simplification: $\dot{\theta_1} = 0 = \Delta\dot{\phi}^{(n)}$ with: $\tilde{\omega} \equiv \omega$. The precession angle θ_{1_0} then becomes a *constant of the motion* given by:

$$\tan^2\theta_{1_0} = \frac{N_p^2}{P_{1_0}^2 + (Q_{1_0}\cos\theta_{1_0})^2}. \quad (22)$$

with $Q_{1_0} = -\alpha\omega$ and:

$$P_{1_0} = -\omega + \gamma B_0\cos\beta_0' + \frac{\gamma}{M_s\sin\theta_{1_0}}\frac{\partial F_{AD_0}}{\partial\theta_1}.$$

Note that F_{AD_0} is the sum over all terms $F_{AD_{\ell m}}(\theta_1,\phi_1)$ with $m = 0$ because the steady-state precession angle cannot depend on the azimuthal angle ϕ_1 that would be time-dependent. This makes sense only in a system with cylindrical symmetry around the precession axis. Obviously, both $\Delta F_Z^{(1)}(B_0, b_p; \omega t)$ and $\Delta F_Z^{(2)}(b_p; 2\omega t)$ are also expected to vanish. Furthermore, one should preferably select a microwave frequency ω high enough to ensure that the condition $B_u/B_0 \ll 1$ will cause $\beta_0' = \theta_{eq}' \to 0$. This means that the approximation of a circularly polarized pump field of half strength should be valid.

Bertotti et al. [48,49] pointed out that, under such conditions, the LLG equation admitted *exact time-harmonic solutions* (called P-modes) with no generation of higher order harmonics in spite of the non-linear character of the LLG equation: in such modes, the magnetization is rigidly rotating with the microwave field and the precession trajectory is circular. Equation (22), which describes an ideal, circular precession, should be a good approximation for XDMR in a YIG film grown on a (111) GGG substrate when $\mathbf{H_0}$ is perpendicular to the film. Since $\beta_0' = \theta_{eq}' = 0$, $P_{1_0} \to P_0$ with:

$$P_0 = \Delta_\omega + \gamma\left[B_u - \frac{2}{3}B_{A1}\left(1 - \frac{7}{4}\sin^2\theta_0'\right)\right]\cos\theta_0'$$

in which the notation: $\Delta_\omega = -\omega + \gamma B_0$ was introduced for brevity. Here, we simply ignored the (weak) trigonal anisotropy term $\propto A_{43}''\sin 3\phi$ which would have broken cylindrical symmetry. Defining next: $b_{cp} = b_{lp}/2$, one may write:

$$\tan^2\theta_0' = \frac{(\gamma b_{cp})^2}{P_0^2 + (Q_0\cos\theta_0')^2} \quad (23)$$

$$\tan\Psi_{1_0} = \tan\phi_{1_0} = \frac{Q_0\cos\theta_0'}{P_0}. \quad (24)$$

Equations (23, 24) allowed Gnatzig, Dötsch et al. [10] to analyze their ODMR experiments. In the low microwave power limit, i.e. when $\cos\theta_0' \to 1$, the resonance condition $P_0 = 0$ will obviously converge towards the standard FMR result whereas $\phi_{1_0} \to \pi/2$ if $P_0 \to 0$.

Equations (23, 24) should still keep sense even though the precession trajectory is not rigorously circular. It is required, however, to stay within limits compatible with a weak perturbation of the P-modes [49]. In such an *extended* steady-state regime, one would access to a *time-averaged* precession cone $\overline{\theta_0'} = \theta_{1_0}$. This regime should typically accommodate the small perturbation due to the weak trigonal anisotropy $\propto A_{43}''\sin 3\phi$ as discussed above. It should accommodate as well small inclination angles, i.e. in the limit $\beta' \to 0$. In the latter case, we propose to replace empirically Q_{1_0} with: $Q_{1_0}' = -\alpha\omega - \gamma\Delta H_{inh}$ in order to account for some inhomogeneous broadening due to elliptical distortions. Here, ΔH_{inh} could be determined either experimentally using standard FMR spectra or from equation (13).

Neglecting any cubic anisotropy field (B_{A1}) and starting with reasonable guesses for the uniaxial anisotropy field B_u and the Gilbert damping parameter α, we could calculate θ_0' by solving numerically equation (23) as a quartic equation in $\cos\theta_0'$. An iterative perturbation procedure allowed us to take into account cubic anisotropy fields and to refine the determination of the averaged precession angle. Numerous field-swept spectra $\theta_0'(B_0)$ were simulated for a variety of samples and geometries. To simulate the spectra displayed in Figure 3 we injected in our calculation the parameters of a real YIG film grown by liquid phase epitaxy (LPE) on a (111) GGG substrate.

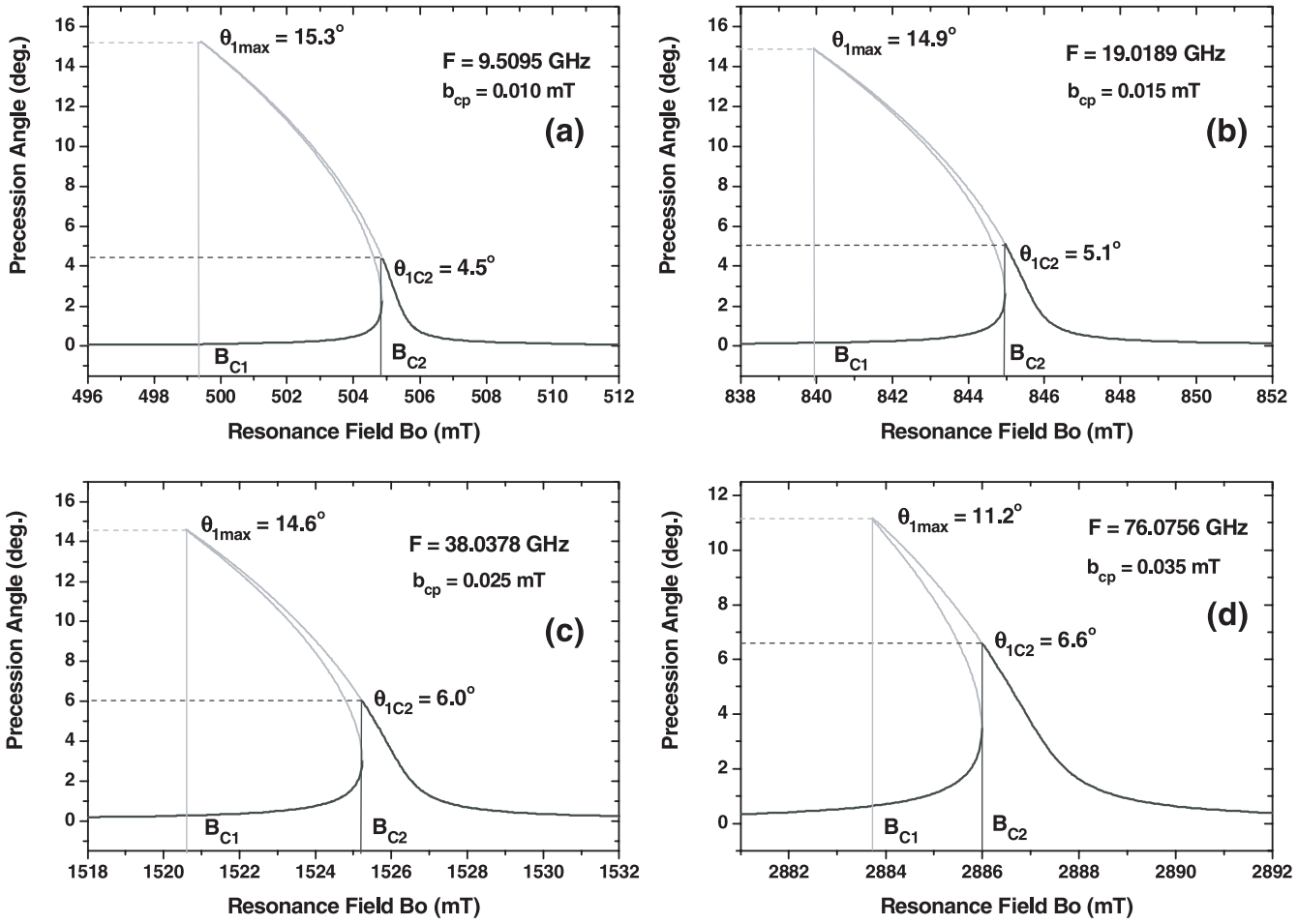

Fig. 3. Simulated field-swept spectra $\theta_0'(B_0)$ for a perpendicularly magnetized YIG film. For microwave frequencies (**F**) raised from 9.51 GHz (a), to 19.0 GHz (b), 38.0 GHz (c) and 76.0 GHz (d), the microwave field b_{cp} was increased from 0.010 mT (a), to 0.015 mT (b), 0.025 mT (c) and 0.035 mT (d). The multi-valued part (or upper branch) of the spectrum comprised between $B_{C1}(\theta_{1max})$ and $B_{C2}(\theta_{1C2})$ cannot be scanned experimentally when the microwave power is amplitude modulated.

Standard FMR spectra were recorded at 9.51 GHz with $\mathbf{H_0}$ perpendicular to the film: the resonance field allowed us to determine $B_u - 2/3B_{A1} \simeq 165$ mT, whereas the FMR linewidth ($\Delta H_{fwhm} = 0.7$ Oe) was found consistent with a very low damping factor: $\alpha \simeq 6 \times 10^{-5}$ and $\Delta H_{inh} \simeq 0.35$ Oe. As illustrated with Figure 3, the angular precession spectra simulated with equation (23) systematically exhibit foldover lineshapes as predicted by Weiss [20]. Note that these simulations refer to only modest microwave fields ($b_{cp} \leq 0.035$ mT) while the pump frequency was raised up to 76 GHz.

2.5 Critical thresholds

A key parameter for XDMR is the maximum angle of precession θ_{1max} at resonance, i.e. when $P_{1_0} = 0$. From equation (22) one obtains:

$$\sin\theta_{1max} = \frac{1}{2}[\cos^2\beta_0'\cos^2\alpha_0' + \sin^2\alpha_0']^{1/2}\frac{(\gamma b_{lp})}{\alpha\omega_0}. \quad (25)$$

At high microwave frequency, i.e. when $\beta_0' = \theta_{eq}' \simeq 0$ and $b_{cp} = b_{lp}/2$, equation (25) can be simplified:

$$\sin\theta_{1max} = \frac{(\gamma b_{cp})}{\alpha\omega_0} \simeq \frac{b_{cp}}{B_0}[\alpha]^{-1}.$$

In the *linear* regime of FMR relaxation at very low microwave power, the damping parameter α can be related either to the linewidth ΔH, to the BB longitudinal (T_1) or transverse (T_2) relaxation times, or to the probability of destruction of $k = 0$ magnons [39]:

$$\alpha\omega_0 = \frac{\gamma\Delta H}{2} = \frac{1}{T_2} = \frac{1}{2T_1} + \frac{1}{T_D} = \frac{\lambda_{0k} + \lambda_{0\sigma}}{2}. \quad (26)$$

Clearly, T_1 and T_2 become different for finite values of T_D which is accounting (artificially) for the contribution of extrinsic processes, e.g. magnon-magnon scattering processes. From the linewidth definition:

$$\sin\theta_{1max} = \frac{2b_{cp}}{\mu_0\Delta H} = \frac{2b_{cp}}{\mu_0\sqrt{3}\Delta H_{pp}}.$$

Here, ΔH_{pp} denotes the (peak-to-peak) FMR linewidth measured at the inflexion points, assuming Lorentzian lineshapes and again low microwave power. For a circularly polarized pump field, the condition $\sin\theta_{1max} \leq 1$ would yield the following *saturation* field most often expressed in terms of the BB relaxation times:

$$h_{cp_{sat}} \leq \frac{\sqrt{2}}{2\sqrt{\gamma^2 T_1 T_2}}.$$

As underlined by Gnatzig, Dötsch et al. [10] and others [47], θ_{1max} can never be reached when the microwave power is amplitude modulated at low frequency because it is impossible to scan the upper branch of the foldover lineshape comprised between the two critical fields B_{C1} and B_{C2} marked in Figure 3 and where the slope of the spectrum becomes infinite. The largest precession angle compatible with XDMR experiments is thus only θ_{1C2} which can be determined numerically. As illustrated with Figure 3, the ratio $\rho = \theta_{1C2}/\theta_{1max}$ also drops down rapidly when the FMR lines become very narrow with the practical consequence that the benefit of decreasing the microwave frequency gets spoiled. The foldover regime could be characterized by the extent to which the two critical fields B_{C1} and B_{C2} are split. Bertotti et al. [48] pointed out that the foldover regime resulted from the co-existence of four P-modes, only two of them being stable. This allowed them to calculate analytically the exact threshold field b_{fold} for foldover:

$$\frac{b_{fold}^2}{(\mu_0 M_s)^2} = \frac{4(\alpha\hat{\omega})^3}{|\kappa_{eff}|} \frac{\sqrt{1+\Omega^2}}{(\sqrt{1+\Omega^2}+|\Omega|)^2} \qquad (27)$$

in which: $\hat{\omega} = \omega/\gamma M_s$, $\Omega = \alpha\hat{\omega}/\kappa_{eff}$, whereas $\kappa_{eff} = B_u/\mu_0 M_s$. Approximate formulas of Anderson and Suhl [50] or Skrotskii and Alimov [51] yield close-lying threshold fields. For the YIG film magnetized perpendicularly and discussed in Section 2.4, the foldover threshold is quite low: $b_{fold} = 0.00045$ mT at $\mathbf{F} = 9.51$ GHz. With such a low threshold, the nonlinear regime is reached very rapidly and makes standard FMR analyses irrelevant. Let us emphasize that XDMR experiments should be performed with microwave fields well beyond b_{fold} (see Fig. 3 for illustration). Indeed, the apparent lineshapes measured under such conditions have no more direct physical meaning: only the experimental determination of the critical jump B_{C2} is of practical interest.

We deliberately ignored so far the contribution of nonlinear terms that couple the uniform mode to higher order magneto-exchange modes or spin waves [18,21,28]. In 1959, Suhl predicted that the precession angle could hardly exceed another threshold value θ_{1S} beyond which parametric amplification of spin-waves could also cause *foldover-like* FMR lineshapes [52,53]. It is well documented that θ_{1S} may be quite different for ferromagnetic thin films magnetized either tangentially or perpendicularly. For circular precession in perpendicularly magnetized films, the first order instability predicted by Suhl can cause only a *subsidiary* microwave absorption off-resonance since resonance occurs at the bottom of the magnon band, far above $\omega/2$. Under such conditions, θ_{1S} will refer to a 2nd order instability process: the annihilation of two magnons is a process which changes the norm of the magnetization vector M_s but occurs only at extremely high microwave power [54]. In other terms, the steady-state precession model developed in Section 2.4 for a ferromagnetic thin film with the magnetization perpendicular to the film should be reasonably safe to analyze XDMR spectra.

With tangentially magnetized films, the Suhl instability threshold occurs at much lower microwave power. Nevertheless, the situation should not be desperate since it was predicted by Suhl himself [55] that the instability threshold could be substantially raised using either field or frequency modulation techniques [56,57]. As noted by Nibarger et al. [58], the instability threshold could be also increased in PIM experiments carried out in the time-domain due to *incoherent* excitation of spinwaves. There is, however, the major complication that the precession is elliptic: this problem will be addressed in a forthcoming paper [19].

3 Information content of XDMR

3.1 Normalized XDMR cross sections

In this section, we focus onto the model of *steady-state* precession around the direction of $\mathbf{M}_{eq}$. As far as the length of the precessing magnetization can be regarded as truly invariant, the following change ΔM_{Z_1} of the axial magnetization is to be expected:

$$\Delta M_{Z_1} = M_s[\cos\theta_{1_0} - 1] \simeq -\frac{1}{2}\tan^2\theta_{1_0}\left(1 - \frac{3}{4}\tan^2\theta_{1_0} + ...\right)M_s \qquad (28)$$

Indeed, we are also interested in the oscillating transverse components:

$$\Delta M_{\perp u_1} = -\sqrt{2}u_{11}(\theta_{1_0},\phi_1)M_s = \sin\theta_{1_0}\cos\phi_1 M_s$$
$$\Delta M_{\perp v_1} = -\sqrt{2}v_{11}(\theta_{1_0},\phi_1)M_s = \sin\theta_{1_0}\sin\phi_1 M_s \qquad (29)$$

Since the precession angles θ_{1_0} are most often small, ΔM_{Z_1} is only a 2nd order effect compared to $\Delta M_\perp$ because: $\sin\theta_{1_0} \simeq \tan\theta_{1_0}[1 - \frac{1}{2}\tan^2\theta_{1_0} + ...]$.

Whereas the model of wide-angle precession of Section 2.3 referred to the precession frame (X_1, Y_1, Z_1), XMCD cross-sections have ultimately to be calculated with respect to the laboratory axes (X', Y', Z'). We need therefore to project onto the latter axes not only the equilibrium magnetization $\mathbf{M}_{eq}$ which is responsible for the *static* XMCD, but also the time-invariant component $\mathbf{\Delta}M_{Z_1}$ and the oscillating transverse components $\mathbf{\Delta}M_\perp$. This was achieved using equation (16) of Section 2.3 and the relevant Wigner D-functions. Indeed, the case of a ferromagnetic film with uniaxial anisotropy and perpendicular magnetization is once again trivial because $(\alpha'_0,\beta'_0,\gamma'_0) \to 0$. In the perspective of future extensions of

the present theory to include weakly elliptic precession, we tried to keep a formulation of XDMR cross-sections as general as possible, i.e. with $(\alpha'_0,\beta'_0,\gamma'_0) \neq 0$. We found anyhow attractive to normalize systematically the XDMR cross-sections with respect to the *static* (equilibrium) XMCD cross-sections measured in strictly the same geometry and under the same conditions.

In the longitudinal geometry of Figure 1, i.e. $\mathbf{k_x} = \mathbf{k}_\parallel$, the non-oscillating component $\Delta M_{Z'}$ leads to:

$$\frac{\Delta\sigma_{XDMR}(k_\parallel)}{[\Delta\sigma_{XMCD}(k_\parallel)]_{eq}} = (\cos\theta_{1_0} - 1) \simeq -\frac{1}{2}\tan^2\theta_{1_0} \quad (30)$$

in which the $\cos\beta'_0$ factors cancel out. Whenever the equilibrium magnetization ($\mathbf{M}_{eq}$) will depart from the direction of the static bias field ($\mathbf{B}_0$), one should detect an additional XDMR signal oscillating at the microwave frequency ω along Z':

$$\frac{\Delta\sigma_{XDMR}(k_\parallel;\omega t)}{[\Delta\sigma_{XMCD}(k_\parallel)]_{eq}} \simeq -\tan\beta'_0\tan\theta_{1_0}\cos(\phi_1+\gamma'_0). \quad (31)$$

This signal being $\propto \tan\beta'_0$, vanishes for a ferromagnetic film with perpendicular magnetization and true uniaxial anisotropy. It will grow, however, as soon as the sample is inclined or rotated ($\beta', \beta'' \neq 0$) and a situation in which: $\tan\beta'_0 \simeq \tan\theta_{1_0}$ is not irrealistic.

In the transverse geometry, i.e. $\mathbf{k_x} = \mathbf{k}_\perp$, the projection along X' of the oscillating components $\Delta M_\perp$ is:

$$\Delta M_{X'} \simeq \tan\theta_{1_0} M_s \times [\cos\beta'_0\cos\alpha'_0\cos(\phi_1+\gamma'_0) - \sin\alpha'_0\sin(\phi_1+\gamma'_0)] \quad (32)$$

whereas the projection along Y' is:

$$\Delta M_{Y'} \simeq \tan\theta_{1_0} M_s \times [\cos\beta'_0\sin\alpha'_0\cos(\phi_1+\gamma'_0) + \cos\alpha'_0\sin(\phi_1+\gamma'_0)]. \quad (33)$$

As expected for the projection of any circular precession trajectory, equations (32,33) describe a weakly elliptical precession trajectory in the (X', Y') plane. Thus, for a transverse XDMR signal measured along Y' one obtains the following normalized cross-sections:

$$\frac{\Delta\sigma_{XDMR}(k_\perp;\omega t)}{[\Delta\sigma_{XMCD}(k_\parallel)]_{eq}} \simeq \tan\theta_{1_0} \times [\sin\alpha'_0\cos(\phi_1+\gamma'_0) + \frac{\cos\alpha'_0}{\cos\beta'_0}\sin(\phi_1+\gamma'_0)]. \quad (34)$$

Whenever the equilibrium magnetization ($\mathbf{M}_{eq}$) will depart from the direction of the static bias field ($\mathbf{B_0}$), there should be also a very weak non-oscillating signal along Y':

$$\frac{\Delta\sigma_{XDMR}(k_\perp)}{[\Delta\sigma_{XMCD}(k_\parallel)]_{eq}} \simeq -\frac{1}{2}\tan\beta'_0\sin\alpha'_0\tan^2\theta_{1_0}. \quad (35)$$

This signal should be extremely weak because both $\tan\beta'_0$ and $\sin\alpha'_0$ are small whereas $\tan^2\theta_{1_0}$ is itself a second order effect.

Equations (30, 34) lead to the remarkable conclusion that, on combining XDMR and XMCD measurements properly, one could determine reliably the steady-state precession angles *locally*, i.e. directly at the X-ray absorbing sites. Remember that it is never a trivial task to determine the *effective* precession angles using conventional FMR experiments because: (i) the exact value of b_p is poorly known at the sample location, i.e. inside a microwave resonator or on a microstrip circuit; (ii) radiation damping effects can only be crudely estimated; (iii) it is difficult to disentangle which are the relevant contributions to the linewidth.

Notice that the oscillating components $\Delta\sigma_{XDMR}(\omega t)$ vary linearly with the microwave induction b_p whereas the non-oscillating components $\Delta\sigma_{XDMR}$ are proportional to the microwave power $\propto b_p^2$. This has the important implication that the non-oscillating longitudinal component $\Delta\sigma_{XDMR}$ is a true time-reversal *odd* property which should change its sign when $\mathbf{B_0}$ is reverted independently of the sign of $\mathbf{b_p}$. Only *normalized* cross sections are insensitive to time-reversal: this is why equation (30) yields a phase-independent, steady-state precession angle.

3.2 Ellipticity of precession

In FMR, the precession ellipticity is defined as [21]:

$$\mathcal{E} = 1 - \frac{|\Delta M_{\perp min}|^2}{|\Delta M_{\perp max}|^2} \quad (36)$$

which does not imply that the trajectory had to be a planar ellipse. Indeed, $\mathcal{E}$ vanishes for a true steady-state circular precession caused by a circularly polarized microwave field in a ferromagnetic thin film satisfying the criteria of cylindrical symmetry of Section 2.4. In contrast, a ferromagnetic thin film magnetized tangentially, will systematically exhibit an elliptic precession caused primarily by the uniaxial anisotropy field B_u.

Let us anticipate that in a near future, it will become attractive to determine *locally* the ellipticity of the precession trajectory. Let us also emphasize that the magnetic ellipticity is a time-reversal *even* property of the system which involves squared transverse components of the magnetization. It may then be preferable to select an X-ray probe that would be directly sensitive to the square of the magnetization. This is possible if we replace the incident circularly polarized X-rays with linearly polarized X-rays, i.e. if we substitute X-ray Magnetic Linear Dichroism (XMLD) to XMCD. This would be a direct transposition in the X-ray regime of a peculiar ODMR experiment performed by Venitskii et al. [8] at optical wavelengths: these authors measured the precession ellipticity in a single crystal of YIG using the magnetic birefringence of the crystal, i.e. the Cotton-Mouton effect. The advantage of XDMR would lay in the element/edge selectivity of the X-ray probe as emphasized in the next sections. Note that the detection geometry would look rather unusual for XMLD measurements since, in XDMR, the X-ray wavevector should be colinear with the static bias field

$\mathbf{B_0} = \mu_0 \mathbf{H_0}$ and not perpendicular to it as this is required for conventional static XMLD measurements.

Squaring a transverse magnetization component $\Delta M_\perp$ oscillating at the microwave frequency ω will result into a steady-state (non-oscillating) component proportional to the microwave power ($\propto b_p^2$) plus another term oscillating at twice the microwave frequency. If the microwave power is square modulated at low frequency, synchronous detection should allow us to extract a very weak steady-state XMLD signal from the intense background associated with the X-ray absorption cross section. The precession ellipticity would then be obtained in rotating the linear polarization of the incident X-ray, e.g. using an X-ray quarter-wave plate. This approach would benefit from the advantage that, again, no fast X-ray detection electronics would be needed. Unfortunately, the XMLD probe is much less sensitive than XMCD and the insertion losses of a quarter-wave plate will spoil the X-ray photon flux: thus, it looks today like a formidable challenge to achieve the huge dynamic range required for such measurements.

There is another experimental approach which may deserve attention if a fast X-ray detection system becomes soon operational: keeping XMCD as a probe, we may try to detect directly the harmonic distortion of the precession trajectory producing a longitudinal component $\Delta M_{Z'}$ oscillating at twice the microwave frequency [18], not to be confused with the signal of equation (31). This approach exploiting the non-linear character of the LLG equation will be envisaged in a forthcoming paper [19]. It should be technically most relevant at low microwave frequencies (e.g. in the L or S bands), with the advantage that the lower resonant bias field would increase the ratio B_u/B_0 in equation (10) and thus maximize the ellipticity of the precession trajectories.

3.3 XDMR at a K-edge

It is a quite remarkable peculiarity of XMCD and XDMR experiments carried out at a K-edge that the effective operators responsible for X-ray circular dichroism are purely of *orbital* nature. This is obvious if one refers to the (historical) *two-step* model of XMCD [1]. Recall that the first step would be an atomic Fano effect. In the absence of spin-orbit coupling in the $1s$ core state, the angular momentum carried by the absorbed X-ray photon is entirely converted into *orbital* polarization of the ejected photoelectron. However, the empty final states *are* spin-polarized: spin-orbit coupling appears then as the primary cause of the orbital polarization responsible for XMCD. This was elegantly summarized in the orbital sum-rule [1]:

$$\int \frac{dE_{\mathbf{x}}}{\hbar\omega_{\mathbf{x}}}[\Delta\sigma_{j+} + \Delta\sigma_{j-}] = \frac{3}{\ell}\Omega_\ell \langle L_z \rangle_\ell \qquad (37)$$

in which $\Delta\sigma_{j\pm}$ denotes the X-ray absorption cross-sections for the core states $j\pm = c \pm 1/2$; Ω_ℓ denotes here the absorption cross-section *per* hole of symmetry ℓ in the valence band and can be viewed as a constant for a given atom and a given edge. At K-edges, we have $c = 0$ and for $3d$ transition metals, the final state are $4p$ orbitals ($\ell = 1$).

In the XDMR experiment of reference [14], the sample was a YIG ($Y_3Fe_5O_{12}$) thin film and the weak Fe K-edge XDMR signal allowed us to probe the precession of selected orbital magnetization components at the iron sites. Since the energy of the X-ray monochromator was kept fixed at the maximum of the dichroism, it is more appropriate to exploit a differential formulation of equation (37) as proposed by Strange or Ebert and others [3–5]:

$$\Delta\sigma_K = 3\Omega_1 \frac{d}{d\Delta E_{\mathbf{x}}} \langle L_z \rangle_p = 3\Omega_1 \langle \ell_z \rangle_p \qquad (38)$$

in which $\Delta E_{\mathbf{x}} = E_{\mathbf{x}} - E_F$ is the energy of the photoelectron referred to the Fermi level. The effective operator appearing in the left handside of equation (38) defines the orbital polarization of p-projected densities of states (DOS) in the valence band. For brevity, we may call it *orbital magnetization* DOS.

One should keep in mind that equations (37) and (38) were established for $1s \rightarrow 4p$ electric dipole ($E1$) transitions. Since the maximum of the XMCD signal was found in the pre-edge region of the X-ray Absorption Near Edge Structures (XANES), one could envisage a small contamination of the XMCD spectrum by $1s \rightarrow 3d$ electric quadrupole ($E2$) transitions. Carra et al. [2] have also proposed an integral sum-rule for the $E2$ transitions at a K-edge:

$$\int \frac{dE_{\mathbf{x}}}{(\hbar\omega_{\mathbf{x}})^2}[\Delta\sigma_{j+} + \Delta\sigma_{j-}]_{(E2)} \propto \frac{1}{50}\{\langle L_z \rangle_{3d} + \frac{1}{3}(5\cos^2\vartheta - 3)\langle O_{zzz} \rangle_{3d}\}\cos\vartheta \qquad (39)$$

in which $\langle O_{zzz} \rangle_{3d}$ is a component of a pure orbital octupolar tensor [2]. Recall that this tensor should anyhow vanish in a cubic crystal field, at least in the absence of any magnetic bias field. At this stage, the important message is that we can extend to quadrupolar transitions our initial statement that no effective spin operator is directly involved in XMCD at a K-edge. Indeed, as emphasized by Guo [5], the orbital magnetization DOS would vanish either if no spin-orbit coupling would exist in the final state, or if no spin-polarization of the empty state occurred.

3.4 XDMR at spin-orbit split L-edges

XMCD signals are known to be much more intense at spin-orbit split L-edges, especially when the XANES spectra exhibit strong *white* lines. This is true in the soft X-ray range where the XMCD signals recorded at the L-edges of $3d$ transition metals are typically two orders of magnitude more intense than the XMCD signals recorded at the K-edge of the same element. This is a formidable advantage in favour of soft-XDMR experiments, but it is partly counter-balanced by serious complications in the exploitation of the XDMR spectra. The reason is that it becomes much more speculative to disentangle the precessional dynamics of the spin and orbital magnetization components. Indeed, equation (37) still holds true for the

$2p \rightarrow nd$ ($E1$) transition ($\ell = 2$), but $\Delta\sigma_{j+}$ and $\Delta\sigma_{j-}$ now refer to absorption cross-sections measured respectively at L_{III} and L_{II} edges. In practice, it is never a trivial exercise to combine accurately XMCD signatures recorded at the L_{III} and L_{II} edges because: (i) one needs to couple together measurements referring to strictly the same energy $\Delta E_{\mathbf{x}} = E_{\mathbf{x}} - E_F$ of the photoelectron; (ii) the XMCD signals should be carefully normalized to the relevant edge jumps $\sigma_{0_{j+}}$ and $\sigma_{0_{j-}}$. As far as these difficulties can be overcome, then, one may exploit again the differential formulation of the sum-rules to derive the following equations:

$$\frac{\Delta\sigma_{L_{III}}}{\sigma_{0_{j+}}} = \frac{C_d}{3N_b}\frac{d}{d\Delta E_{\mathbf{x}}}\{\langle L_z\rangle_d + \frac{2}{3}\langle S_z\rangle_d + \frac{7}{3}\langle T_z\rangle_d\}$$
$$= \frac{C_d}{3N_b}\{\langle \ell_z\rangle_d + \frac{2}{3}\langle s_z\rangle_d + \frac{7}{3}\langle t_z\rangle_d\} \quad (40)$$
$$\frac{\Delta\sigma_{L_{II}}}{\sigma_{0_{j-}}} = \frac{C_d}{6}\frac{d}{d\Delta E_{\mathbf{x}}}\{\langle L_z\rangle_d - \frac{4}{3}\langle S_z\rangle_d - \frac{14}{3}\langle T_z\rangle_d\}$$
$$= \frac{C_d}{6}\{\langle \ell_z\rangle_d - \frac{4}{3}\langle s_z\rangle_d - \frac{14}{3}\langle t_z\rangle_d\} \quad (41)$$

in which N_b would be the branching ratio and C_d a constant factor. Selecting $N_b \simeq 2$ would make equation (40) consistent with the (commonly accepted) statistical limit of the branching ratio. Unfortunately, it is well documented that quite significant deviations from the statistical limit are to be expected (and were observed) due to spin-orbit coupling in the final state. Refined estimates of N_b and C_d should be obtained on combining very accurate XMCD measurements over the whole XANES range together with ab initio simulations of static XMCD spectra: this is a stringent pre-requisite to exploit XDMR experiments at spin-orbit split edges.

A priori, XDMR data collected at the L_{III} and L_{II} edges could provide us simultaneously with information regarding the precession dynamics of the *spin* and *orbital* magnetization of d-DOS. In equations (40,41), there is an additional contribution of a peculiar dipole magnetization DOS, i.e. $d\langle T_z\rangle_d/dE$, which reflects (to the lowest order) the asphericity of the spin magnetization due to spin-orbit interactions or anisotropic charge distribution. In practice, the expectation value of $\langle T_z\rangle$ should be much smaller than the spin magnetization $\langle S_z\rangle$ and its contribution is often neglected. As far as XDMR is concerned, $\langle T_z\rangle$ should marginally affect the norm of the precessing spin magnetization in equations (28, 30) and will be neglected below. If we now inject equations (40, 41) into equation (30) and extend simultaneously the definition of ΔM_{Z_1} to each individual magnetization DOS component, i.e. $\langle s_z\rangle_d$ and $\langle \ell_z\rangle_d$, one obtains a set of coupled equations:

$$\{\langle \ell_z\rangle_d + \frac{2}{3}\langle s_z\rangle_d\}[\tan^2\theta_{1_0}]_{L_{III}} = \langle \ell_z\rangle_d \tan^2\theta_{\ell 1_0} + \frac{2}{3}\langle s_z\rangle_d \tan^2\theta_{s1_0} \quad (42)$$

$$\{\langle \ell_z\rangle_d - \frac{4}{3}\langle s_z\rangle_d\}[\tan^2\theta_{1_0}]_{L_{II}} = \{\langle \ell_z\rangle_d\}\tan^2\theta_{\ell 1_0} - \frac{4}{3}\{\langle s_z\rangle_d\}\tan^2\theta_{s1_0} \quad (43)$$

in which θ_{s1_0} and $\theta_{\ell 1_0}$ denote the precession angles of the spin and orbital magnetization DOS which we are most interested in, whereas $[\theta_{1_0}]_{L_{III}}$ and $[\theta_{1_0}]_{L_{II}}$ refer to the *effective* precession angles one would measure experimentally at the relevant L-edge using equation (30). Further simplification is possible on introducing the ratio $\eta = \langle \ell_z\rangle_d/2\langle s_z\rangle_d$ that can be most easily determined experimentally from XMCD measurements:

$$(1+3\eta)[\tan^2\theta_{1_0}]_{L_{III}} = \tan^2\theta_{s1_0} + 3\eta\tan^2\theta_{\ell 1_0} \quad (44)$$
$$(2-3\eta)[\tan^2\theta_{1_0}]_{L_{II}} = 2\tan^2\theta_{s1_0} - 3\eta\tan^2\theta_{\ell 1_0}. \quad (45)$$

The latter equations show that independent XDMR experiments performed at the L_{III} and L_{II} edges should, in principle, allow us to access to the precession angles of the spin and orbital magnetization of d-projected DOS. Equations (44, 45) could then be viewed as a dynamical extension of the static differential sum-rules. Very recently, we already used these equations to analyze XDMR spectra recorded at the Yttrium L-edges in YIG thin films [59].

3.5 Fictitious spin Hamiltonian revisited

In the early days of FMR, Kittel [60] and Van Vleck [61] stressed the important point that FMR was *not* an atomic spectroscopy and that the torque equation $\dot{\mathbf{J}} = \mathbf{M} \times \mathbf{H}$ did not hold true in a crystalline environment [26]. To some extent, fictitious spin Hamiltonians proved to be an elegant tool to obviate this difficulty. Nevertheless, Kittel concluded one of his early papers on FMR with the remark [60] that, in a microwave absorption FMR experiment, changes in the orbital angular momentum should be undetectable due to compensating changes in the lattice angular momentum. It is the originality of XDMR to combine magnetic resonance with an element specific atomic spectroscopy. As shown in Sections 3.3–3.4, XDMR should let us investigate how precession dynamics affects locally p- or d-projected spin and orbital magnetizations DOS.

There is nevertheless a point which deserves more attention. For a given microwave pumping power, the precession angle can be directly determined from the normalized XDMR cross-section, e.g. using equation (30). One may expect the angular precession frequency to be identical for the spin and orbital magnetization components, but the precession cones can hardly be the same because the gyromagnetic factors for spin (g_S) and orbital moments (g_L) are inherently different. Note that g_S and g_L should affect in the same way *static* XMCD as well as *time-dependent* XDMR measurements. Recall that XMCD sum rules were initially established using atomic multiplets calculations and were found to yield reasonably good estimates for the spin and orbital magnetic moments. As long as static XMCD results prove to be correct, then the precession angles for spin and orbital magnetization should be in the

ratio 2:1 as expected from atomic g factors [14]. This point is nevertheless calling for very careful experimental confirmations, e.g. using equations (44, 45) at L-edges. Unfortunately, very few high quality XMCD data were collected so-far on insulators (and paramagnets) for which one might suspect the crystal field to play a major role and fictitious spin Hamiltonians to be helpful.

Let us also take this opportunity to draw attention onto the fact that the spectroscopic splitting factor g should have not only a magnitude but also a sign characterizing the chirality of the precession: an interesting point raised by Blume et al. [26] was that, in systems with significant orbital contributions, the magnetization could precess in the direction *opposite* to that of the free-electron spin. This was shown to happen at least in rare-earth or actinide compounds (e.g. NpF_6) with fairly large orbital moments. Phase sensitive XDMR experiments carried out in the transverse geometry could perhaps become sensitive to the *absolute* chirality of the precession of spin and orbital magnetization components as a function of the helicity on the incoming X-rays.

Large orbital moments in a ground state manifold will favor a strong orbit-lattice coupling with the consequence that the spin-lattice relaxation time T_1 may become very short and the FMR lineshape desperately broad. In their theory of ferrimagnetic resonance in rare-earth doped iron garnets, Kittel and De Gennes [62,63] pointed out that a fast relaxing mechanism could overdamp (semi-quench) the precession of the magnetization in the captive rare-earth lattice. Van Vleck [24,25], however, supported the alternative view that a slow *longitudinal* relaxation mechanism would still dominate if the splitting of the rare-earth energy levels by crystal or exchange fields was large compared to the resonance frequency. Such systems are known to exhibit giant anisotropy shifts and anisotropic relaxation effects [21,25]. We are back into a situation where dynamical (fictitious) spin Hamiltonians should again help [27,24,25]. Note that Van Vleck also casted serious doubt about the adequacy of using a Gilbert damping factor to represent necessarily complicated spin-lattice coupling effects [24]. Anyhow, one should be prepared to face dramatic sensitivity problems to record XDMR spectra of systems featuring large ground-state orbital moments because the broad FMR lineshapes will restrict the efficiency of any type of microwave pumping process.

3.6 Conclusion

With this paper, we want to draw attention onto the fact that XDMR is not just another exotic way to detect FMR. Given that the microwave power required for an XDMR experiment is *ca.* six orders of magnitude higher than in conventional FMR, this approach would have a limited future. However, we have shown in Section 3 that a combination of XDMR with static XMCD measurement could provide us with a reliable estimation of the average precession cone for selected spin and orbital magnetization components at X-ray absorbing sites. In contrast, standard FMR spectra would yield the average precession angle of an *effective spin* magnetization only: this information, even if it was not heavily spoiled by experimental artefacts, would be of limited interest.

Clearly, what makes XDMR attractive is the element and edge selectivity of the XMCD probe. Unfortunately, it was shown in Section 2 that the resonance condition was poorly element selective, e.g. through either a tiny variation of the spectroscopic splitting factor g, or local variations of the magnetocrystalline anisotropy. Unless a spherically shaped single crystal is used, the contribution of B_{A1} is most often overwhelmed by the uniaxial anisotropy field B_u that is *not* element-dependent since its origin is to be found in the demagnetizing field and interfacial anisotropy fields which are sample and shape dependent. This could be one good reason why Bailey et al. [11] failed to detect any significant phase difference in their experiments carried out at the L-edges of iron and nickel in permalloy.

In contrast, one may expect the *nature* of the precessing moments to be strongly element selective: a problem of considerable interest would be to disentangle the precession dynamics of orbital magnetization components which should be strongly element and edge dependent. In this respect, one may hope that XDMR could yield valuable new information regarding the important problem of orbit-lattice coupling which is driving the whole spin-lattice relaxation mechanisms.

To emphasize the complementarity of FMR and XDMR, let us recall the basic assumption made in FMR, which is that the orbital moment is quenched to the 1st order, spin-orbit being introduced only as a 2nd order perturbation mixing excited states into the ground state [29]. In XDMR, we are concerned with the reverse side of the problem which is to understand how the precession of spin and orbital polarized DOS above the Fermi level can be coupled to the precession of (fictitious) spins in the ground state.

The authors greatly appreciated the constant support of Dr. Y. Petroff. We dedicate this paper *in memoriam* of our colleague and friend Dr. Paolo Carra.

Appendix A: Magnetic anisotropy models

A.1 Uniaxial anisotropy along the [001] crystal axis

Uniaxial anisotropy most often results from growth-induced stress in thin films and occurs naturally in hexagonal crystals. Let us start with the classical power series expansion in $\sin\theta$ [34,40]:

$$\Delta F = K_{u1}\sin^2\theta + K_{u2}\sin^4\theta + ...$$

To obtain ΔF_{AD}, we still need to add the contribution of the demagnetizing energy[34]:

$$\Delta F_{AD} = \Delta F + \frac{\mu_0 M_s^2}{2} D\cos^2\theta$$

where the effective demagnetizing coefficient $D \equiv 1$ only for a film of vanishing aspect ratio. Expanding ΔF_{AD} on real spherical harmonics, one readily obtains the desired coefficients:

$$A'_{20} = -\frac{2}{3}K_{u1}\left[1 + \frac{8}{7}\frac{K_{u2}}{K_{u1}}\right] + \frac{\mu_0}{3}DM_s^2;\ \ A'_{40} = \frac{8}{35}K_{u2}.$$

A.2 Cubic symmetry with tetragonal distortion along the growth direction [001]

Following Heinrich and Cochran [34], the magnetocrystalline anisotropy free energy can be written:

$$\Delta F_{AD} = -K_u\cos^2\theta - \frac{1}{2}K_{1\parallel}\sin^4\theta\ [\cos^4\phi + \sin^4\phi] - \frac{1}{2}K_{1\perp}\cos^4\theta + \frac{\mu_0 M_s^2}{2}D\cos^2\theta.$$

Expanding ΔF_{AD} on a real spherical harmonic basis yields the coefficients:

$$A'_{20} = -\frac{2}{3}K_u\left[1 + \frac{3}{7}\frac{K_{1\perp} - K_{1\parallel}}{K_u}\right] + \frac{\mu_0}{3}DM_s^2$$

$$A'_{40} = -\frac{4}{35}K_{1\perp} - \frac{3}{35}K_{1\parallel};\ \ A'_{44} = -\sqrt{\frac{2}{35}}K_{1\parallel}.$$

A.3 Film grown along a cubic [111] direction

Let us select the following set of unit vectors for the symmetry axes: $\boldsymbol{e_1} = [\bar{1}10]$; $\boldsymbol{e_2} = [\bar{1}\bar{1}2]$; $\boldsymbol{e_3} = [111]$. Using standard coordinate transformations and neglecting irrelevant constant terms, one obtains:

$$\Delta F_{AD} = -K_u\cos^2\theta - \frac{2}{3}K_1\sin^2\theta + \frac{7}{12}K_1\sin^4\theta + \frac{\sqrt{2}}{3}K_1\sin^3\theta\cos\theta\sin 3\phi + \frac{\mu_0 M_s^2}{2}D\cos^2\theta$$

where K_u refers to an uniaxial, growth induced anisotropy. The same result was reported by Farle [40]. Expanding ΔF_{AD} on a real spherical harmonic basis yields the following coefficients:

$$A'_{20} = -\frac{2}{3}K_u + \frac{\mu_0}{3}DM_s^2; A'_{40} = \frac{2}{15}K_1; A''_{43} = -\frac{4}{3}\sqrt{\frac{2}{35}}K_1$$

A.4 Film grown along a cubic [110] direction

If one selects now the following unit vectors for the symmetry axes: $\boldsymbol{e_1} = [\frac{\bar{1}}{\sqrt{2}}\frac{1}{\sqrt{2}}0]$; $\boldsymbol{e_2} = [001]$; $\boldsymbol{e_3} = [\frac{1}{\sqrt{2}}\frac{1}{\sqrt{2}}0]$, one obtains:

$$\Delta F_{AD} = -K_u\cos^2\theta - K_1\sin^2\theta + \frac{3}{2}K_1\sin^2\theta\sin^2\phi + K_1\sin^4\theta - K_1\sin^4\theta\sin^2\phi - \frac{3}{4}K_1\sin^4\theta\sin^4\phi + \frac{\mu_0 M_s^2}{2}D\cos^2\theta$$

with the following spherical coefficients:

$$A'_{20} = -\frac{2}{3}K_u + \frac{\mu_0}{3}DM_s^2$$

$$A'_{40} = \frac{1}{20}K_1; A'_{42} = -\frac{1}{2}\sqrt{\frac{2}{5}}K_1; A'_{44} = -\frac{3}{4}\sqrt{\frac{2}{35}}K_1.$$

Appendix B: Inclined/rotated films

Very often, the sample is either inclined, i.e. rotated by a polar angle β' around the laboratory axis Y', or rotated around the laboratory axis X' by the azimuthal angle β''. We describe below how the spherical coefficients $A'_{\ell m}$ and $A''_{\ell m}$ of Section 2.2 transform under such rotations. This is straightforward using the Wigner D-functions which transform spherical harmonics according to:

$$C_{\ell n}(\theta,\phi) = \sum_m D^{\ell}_{mn}(\alpha',\beta',\gamma')C_{\ell m}(\theta',\phi')$$

in which (θ,ϕ) refer to the symmetry coordinate frame whereas (θ',ϕ') refer to the laboratory frame. The $D^{\ell}_{mn}(\alpha',\beta',\gamma')$ functions are represented by the product of three functions:

$$D^{\ell}_{mn}(\alpha',\beta',\gamma') = e^{-\imath m\alpha'}\ d^{\ell}_{mn}(\beta')\ e^{-\imath n\gamma'}$$

in which $d^{\ell}_{mn}(\beta')$ is a real function whose explicit forms are tabulated elsewhere [43] up to $\ell = 4$.

B.1 Inclined film: polar rotation

For a polar rotation β' around Y', there is the simplification: $\alpha' = \gamma' = 0$. For the uniaxial anisotropy which refers to $A'_{20}C_{20}(\theta,\phi)$, the relevant transformation is:

$$A'_{20}C_{20}(\theta,\phi) = A'_{20}\left\{\frac{1}{2}(3\cos^2\beta' - 1)C_{20}(\theta',\phi') - \sqrt{\frac{3}{2}}\sin 2\beta' u_{21}(\theta',\phi') + \sqrt{\frac{3}{2}}\sin^2\beta' u_{22}(\theta',\phi')\right\}.$$

The cubic anisotropy term of cylindrical symmetry is much more cumbrous:

$$A'_{40}C_{40}(\theta,\phi) = A'_{40}\left\{\frac{1}{8}(3 - 30\cos^2\beta' + 35\cos^4\beta')C_{40}(\theta',\phi') + \frac{\sqrt{5}}{4}\sin 2\beta'(3 - 7\cos^2\beta')u_{41}(\theta',\phi') - \frac{\sqrt{10}}{4}\sin^2\beta'(1 - 7\cos^2\beta')u_{42}(\theta',\phi') - \frac{\sqrt{35}}{4}\sin 2\beta'\sin^2\beta' u_{43}(\theta',\phi') + \frac{\sqrt{70}}{8}\sin^4\beta' u_{44}(\theta',\phi')\right\}.$$

The trigonal component $\propto A''_{43}v_{43}$, which, according to Appendix A.3, is to be expected for a YIG film grown on a (111) GGG substrate, would transform as:

$$\begin{aligned}A''_{43}v_{43}(\theta,\phi) = A''_{43}\Big\{ &\frac{3\sqrt{7}}{4}\sin^2\beta'\cos\beta' v_{41}(\theta',\phi') \\ &-\frac{\sqrt{14}}{4}\sin\beta'(1-3\cos^2\beta')v_{42}(\theta',\phi') \\ &-\frac{1}{4}\cos\beta'(5-9\cos^2\beta')v_{43}(\theta',\phi') \\ &-\frac{\sqrt{2}}{4}\sin\beta'(1+3\cos^2\beta')v_{44}(\theta',\phi')\Big\}.\end{aligned}$$

The tetragonal component $\propto A'_{44}u_{44}$ that is found in the case of thin films grown on a (001) substrate, will transform as:

$$\begin{aligned}A'_{44}u_{44}(\theta,\phi) = A'_{44}\Big\{ &\frac{\sqrt{70}}{16}\sin^4\beta' C_{40}(\theta',\phi') \\ &+\frac{\sqrt{14}}{8}\sin 2\beta'\sin^2\beta' u_{41}(\theta',\phi') \\ &+\frac{\sqrt{7}}{4}\sin^2\beta'(1+\cos^2\beta')u_{42}(\theta',\phi') \\ &+\frac{\sqrt{2}}{8}\sin 2\beta'(3+\cos^2\beta')u_{43}(\theta',\phi') \\ &+\frac{1}{8}(1+6\cos^2\beta'+\cos^4\beta')u_{44}(\theta',\phi')\Big\}.\end{aligned}$$

Finally, let us consider as well the transformation of the quadratic term $A'_{42}u_{42}$ that is involved in the anisotropy free energy of films grown on (110) substrates:

$$\begin{aligned}A'_{42}u_{42}(\theta,\phi) = A'_{42}\Big\{ &\frac{\sqrt{10}}{8}\sin^2\beta'(7\cos^2\beta' \\ &-1)C_{40}(\theta',\phi') \\ &+\frac{\sqrt{2}}{4}\sin 2\beta'(7\cos^2\beta'-4)u_{41}(\theta',\phi') \\ &+\frac{1}{2}(1-6\cos^2\beta'+7\cos^4\beta')u_{42}(\theta',\phi') \\ &-\frac{\sqrt{14}}{4}\sin 2\beta'\cos^2\beta' u_{43}(\theta',\phi') \\ &+\frac{\sqrt{7}}{4}\sin^2\beta'(1+\cos^2\beta')u_{44}(\theta',\phi')\Big\}.\end{aligned}$$

B.2 Rotated film: azimuthal rotation

For an azimuthal rotation β'' around OX', we have $\alpha'' = +\frac{\pi}{2}$ and $\gamma'' = -\frac{\pi}{2}$. The uniaxial anisotropy term $A'_{20}C_{20}(\theta,\phi)$ will transform as:

$$\begin{aligned}A'_{20}C_{20}(\theta,\phi) = A'_{20}\{&\frac{1}{2}(3\cos^2\beta''-1)C_{20}(\theta',\phi') \\ &-\sqrt{\frac{3}{2}}\sin 2\beta'' v_{21}(\theta',\phi') - \sqrt{\frac{3}{2}}\sin^2\beta'' u_{22}(\theta',\phi')\}.\end{aligned}$$

Similarly, the cubic anisotropy term of cylindrical symmetry would transform as:

$$\begin{aligned}A'_{40}C_{40}(\theta,\phi) = A'_{40}\Big\{&\frac{1}{8}(3-30\cos^2\beta'' \\ &+35\cos^4\beta'')C_{40}(\theta',\phi') \\ &+\frac{\sqrt{5}}{4}\sin 2\beta''(3-7\cos^2\beta'')v_{41}(\theta',\phi') \\ &+\frac{\sqrt{10}}{4}\sin^2\beta''(1-7\cos^2\beta'')u_{42}(\theta',\phi') \\ &+\frac{\sqrt{35}}{4}\sin 2\beta''\sin^2\beta'' v_{43}(\theta',\phi') \\ &+\frac{\sqrt{70}}{8}\sin^4\beta'' u_{44}(\theta',\phi')\Big\}.\end{aligned}$$

The trigonal component $A''_{43}v_{43}$ would transform as:

$$\begin{aligned}A''_{43}v_{43}(\theta,\phi) = A''_{43}\Big\{ &-\frac{\sqrt{35}}{4}\sin^3\beta''\cos\beta'' C_{40}(\theta',\phi') \\ &+\frac{\sqrt{7}}{4}\sin^2\beta''(1-4\cos^2\beta'')v_{41}(\theta',\phi') \\ &+\frac{\sqrt{14}}{2}\sin\beta''\cos^3\beta'' u_{42}(\theta',\phi') \\ &-\frac{3}{4}(1-\cos^2\beta''-\frac{4}{3}\cos^4\beta'')v_{43}(\theta',\phi') \\ &+\frac{\sqrt{2}}{4}\sin\beta''\cos\beta''(3+\cos^2\beta'')u_{44}(\theta',\phi')\Big\}.\end{aligned}$$

Regarding the tetragonal component $A'_{44}u_{44}$, one would obtain:

$$\begin{aligned}A'_{44}u_{44}(\theta,\phi) = A'_{44}\Big\{ &\frac{\sqrt{70}}{16}\sin^4\beta'' C_{40}(\theta',\phi') \\ &+\frac{\sqrt{14}}{8}\sin 2\beta''\sin^2\beta'' v_{41}(\theta',\phi') \\ &-\frac{\sqrt{7}}{4}\sin^2\beta''(1+\cos^2\beta'')u_{42}(\theta',\phi') \\ &-\frac{\sqrt{2}}{8}\sin 2\beta''(3+\cos^2\beta'')v_{43}(\theta',\phi') \\ &+\frac{1}{8}(1+6\cos^2\beta''+\cos^4\beta'')u_{44}(\theta',\phi')\Big\}\end{aligned}$$

whereas the quadratic term $A'_{42}u_{42}$ will transform as:

$$\begin{aligned}A'_{42}u_{42}(\theta,\phi) = A'_{42}\Big\{ &\frac{\sqrt{10}}{8}\sin^2\beta''(1-7\cos^2\beta'')C_{40}(\theta',\phi') \\ &-\frac{\sqrt{2}}{4}\sin 2\beta''(7\cos^2\beta''-4)v_{41}(\theta',\phi') \\ &+\frac{1}{2}(1-6\cos^2\beta''+7\cos^4\beta'')u_{42}(\theta',\phi') \\ &-\frac{\sqrt{14}}{4}\sin 2\beta''\cos^2\beta'' v_{43}(\theta',\phi') \\ &-\frac{\sqrt{7}}{4}\sin^2\beta''(1+\cos^2\beta'')u_{44}(\theta',\phi')\Big\}.\end{aligned}$$

B.3 Rotated-inclined film

For the sake of brevity, we shall consider only the transformation of the uniaxial anisotropy term in successive rotations (β', β''):

$$\begin{aligned} A'_{20}C_{20}(\theta,\phi) = A'_{20}\{&\frac{1}{2}(3\cos^2\beta'\cos^2\beta'' - 1)\ C_{20}(\theta',\phi') \\ &-\sqrt{\frac{3}{2}}[\sin 2\beta'\cos\beta''\ u_{21}(\theta',\phi') \\ &+\sin 2\beta''\cos^2\beta'\ v_{21}(\theta',\phi')] \\ &+\sqrt{\frac{3}{2}}[\ [1+\cos^2\beta'(\cos^2\beta''-2)]u_{22}(\theta',\phi') \\ &+\sin 2\beta'\sin\beta''\ v_{22}(\theta',\phi')]. \end{aligned}$$

References

1. A. Rogalev, F. Wilhelm, N. Jaouen, J. Goulon, J.P. Kappler, *X-ray Magnetic Circular Dichroism*, in *Magnetism: A Synchrotron Radiation Approach*, edited by E. Beaurepaire, H. Bulou, F. Scheurer, J.-P. Kappler, Lecture Notes in Physics **697** (Springer Verlag, Berlin-Heidelberg, 2006), pp. 71–94
2. P. Carra, H. König, B.T. Thole, M. Altarelli, Physica B **192**, 182 (1993)
3. P. Strange, J. Phys.: Condens. Matter **6**, L491 (1994)
4. H. Ebert, Rep. Prog. Phys. **59**, 1665 (1996)
5. G.Y. Guo, J. Phys.: Condens. Matter **8**, L747 (1996)
6. M. Bonfim, G. Ghiringhelli, F. Montaigne, S. Pizzini, N. Brookes, F. Petroff, J. Vogel, J. Camarero, A. Fontaine, Phys. Rev. Lett. **86**, 3646 (2001)
7. J.T. Hanlon, J.F. Dillon, J. Appl. Phys. **36**, 1269 (1965)
8. V.N. Venitskii, V.V. Eremenko, E.V. Matyushkin, Sov. Phys. JETP **40**, 713 (1975)
9. A.S. Borovik-Romanov, N.M. Kreines, R. Laiho, T. Levola, V.G. Zhotikov, J. Phys. C: Solid St. Phys. **13** 879 (1980)
10. K. Gnatzig, H. Dötsch, M. Ye, A. Brockmayer, J. Appl. Phys. **62**, 4839 (1987)
11. W.E. Bailey, L. Cheng, D.J. Keavney, C.-C. Kao, E. Vescovo, D.A. Arena, Phys. Rev. B **70**, 172403 (2004)
12. J. Goulon, F. Sette, W.G. Stirling, in *Emerging Scientific Opportunities at the ESRF*, ESRF Medium-Term Scientific Programme for the period 2003–2007, (2002)
13. G. Boero, S. Rusponi, P. Bencok, R.S. Popovic, H. Brune, P. Gambardella, Appl. Phys. Lett. **87**, 152503 (2005)
14. J. Goulon, A. Rogalev, F. Wilhelm, N. Jaouen, C. Goulon-Ginet, G. Goujon, J. Ben Youssef, M.V. Indenbom, JETP Lett. **82**, 791 (2005)
15. A. Puzic, B. Van Waeyenberge, K.W. Chou, P. Fischer, H. Stoll, G. Schütz, T. Tyliszczak, K. Rott, H. Brückl, G. Reiss, I. Neudecker, T. Haug, M. Buess, C.H. Back, J. Appl. Phys. **97**, 1 (2005)
16. N. Bloembergen, R.W. Damon, Phys. Rev. **85**, 699 (1952)
17. N. Bloembergen, S. Wang, Phys. Rev. **93**, 72 (1954)
18. R.W. Damon, in *Ferromagnetic Resonance at High Power*, edited by G.T. Rado, H. Suhl, Magnetism, Vol. **I**, (Academic Press, New-York, London, 1963), Chap. 11, pp. 551–620
19. J. Goulon et al., *XDMR: Elliptical precession with harmonic distorted trajectories*, (to be published)
20. M.T. Weiss, Phys. Rev. Lett. **1**, 239 (1958)
21. A.G. Gurevich, G.A. Melkov, *Magnetization Oscillations and Waves*, (CRC Press Inc., Boca Raton, 1996)
22. Y.K. Fetisov, C.E. Patton, IEEE Trans. Magnetics **40**, 473 (2004)
23. A. Abragam, M.H.L. Pryce, Proc. Phys. Soc. A **205**, 135 (1951)
24. J.H. Van Vleck, Phys. Rev. **123**, 58 (1961)
25. J.H. Van Vleck, J. Appl. Phys. **35**, 882 (1964)
26. M. Blume, S. Geschwind, Y. Yafet, Phys. Rev. **181**, 478 (1969)
27. R. Orbach, H.J. Stapleton, *Electron Spin-Lattice Relaxation*, edited by S. Geschwind (Plenum Press, New York-London, 1972)
28. A.I. Akhiezer, V.G. Bar'yakhtar, S.V. Peletminskii, *Spin Waves*, edited by C.J. Gorter, R. De Bruyn Ouboter, D. De Klerk (North-Holland Series in Low Temperature Physics, Vol. **I**, Amsterdam, 1968)
29. A.N. Anisimov, M. Farle, P. Poulopoulos, W. Platow, K. Baberschke, P. Isberg, R. Wäppling, A.M.N. Niklasson, O. Eriksson, Phys. Rev. Lett. **82**, 2390 (1999)
30. Th.L. Gilbert, IEEE Trans. Magn. **40**, 3443 (2004)
31. F.H. Leeuw, R. van den Doel, U. Enz, Rep. Prog. Phys. **43**, 689 (1980)
32. L. Kraus, Z. Frait, J. Schneider, Phys. Stat. Sol. (a) **64**, 449 (1981)
33. B. Heinrich, A.S. Arrott, J. Appl. Phys. **57**, 3709 (1985)
34. B. Heinrich, J.F. Cochran, Advances in Physics, Vol. **42**, 523 (1993)
35. N. Smith, J. Appl. Phys. **92**, 3877 (2002)
36. R.K. Wangsness, Phys. Rev. **98**, 927 (1955)
37. R.C. Fletcher, R.C. LeCraw, E.G. Spencer, Phys. Rev. **117**, 955 (1960)
38. H.B. Callen, E. Pitelli, Phys. Rev. **119**, 1523 (1960)
39. C. Haas, H.B. Callen, *Ferromagnetic Relaxation and Resonance Line Widths*, edited by G.T. Rado, H. Suhl, Magnetism, Vol. **I**, (Academic Press, New-York, London, 1963), Chap. 10, pp. 449–549
40. M. Farle, Rep. Prog. Phys. **61** 755 (1998)
41. J. Miltat, G. Albuquerque, A. Thiaville, *Micromagnetics: Dynamical Aspects*, in *Magnetism and Synchrotron Radiation*, edited by E. Beaurepaire, F. Scheurer, G. Krill, J.-P. Kappler, Lecture Notes in Physics **565**, (Springer Verlag, Berlin-Heidelberg, 2001), pp. 129–56
42. L. Baselgia, M. Warden, F. Waldner, S.L. Hutton, J.E. Drumheller, Y.Q. He, P.E. Wigen, M. Marysko, Phys. Rev. B **38**, 2237 (1988)
43. D.A. Varshalovich, A.N. Moskalev, V.K. Khersonskii, *Quantum Theory of Angular Momentum*, (Word Scientific Publishing Co. Pte Ltd, New York, 1988)
44. J. Smit, H.J. Beljers, Philips Res. Rep. **10**, 113 (1955)
45. H. Suhl, Phys. Rev. **97**, 555 (1955)
46. G.V. Skrotskii, L.V. Kurbatov, Sov. Phys. JETP **35**, 148 (1959)
47. V. Charbois, Ph.D. thesis, University of Paris VII - Denis Diderot, (2003)

48. G. Bertotti, C. Serpico, I.D. Mayergoyz, Phys. Rev. Lett. **86**, 724 (2001)
49. G. Bertotti, I.D. Mayergoyz, C. Serpico, IEEE Trans. Magn. **38**, 2403 (2002)
50. P.W. Anderson, H. Suhl, Phys. Rev. **100**, 1788 (1955)
51. G.V. Skrotskii, Yu. Alimov, Sov. Phys. JETP **36**, 899 (1959)
52. H. Suhl, J. Appl. Phys. **30**, 1961 (1959)
53. H. Suhl, J. Appl. Phys. **31**, 935 (1960)
54. A. Berteaud, H. Pascard, J. Appl. Phys. **37**, 2035 (1966)
55. H. Suhl, Phys. Rev. Lett. **6**, 174 (1961)
56. T.S. Hartwick, E.R. Peressini, M.T. Weiss, Phys. Rev. Lett. **6**, 176 (1961)
57. J.F. Ollom, H.L. Goldstein, J. Appl. Phys. **32**, 2059 (1961)
58. J.P. Nibarger, R. Lopusnik, T.J. Silva, Appl. Phys. Lett. **82**, 2112 (2003)
59. J. Goulon, A. Rogalev, F. Wilhelm, N. Jaouen, C. Goulon-Ginet, G. Goujon, J. Ben Youssef, M.V. Indenbom, J. Electron Spectrosc. Relat. Phenom. submitted (2006)
60. C. Kittel, Phys. Rev. **76**, 743 (1949)
61. J.H. Van Vleck, Phys. Rev. **78**, 266 (1950)
62. C. Kittel, Phys. Rev. **115**, 1587 (1959)
63. P.-G. De Gennes, C. Kittel, A.M. Portis, Phys. Rev. **116**, 323 (1959)
64. C. Kittel, Phys. Rev. **117**, 681 (1960)